

On the Detectability of Turbulence and Bulk Flows in X-ray Clusters[†]

Rashid A. Sunyaev^{1,2}, Michael L. Norman^{1,3}, and Greg L. Bryan⁴

ABSTRACT

Cooling flows, cluster mergers and motions of galaxies through the cluster gas with supersonic and sonic velocities must lead to large scale motions of the intracluster medium (ICM). A high-resolution numerical simulation of X-ray cluster formation by Norman and Bryan predicts cluster-wide turbulence with $v_{turb} \sim 300 - 600$ km/s and eddy scales $l_{outer} \sim 100 - 500$ kpc, the larger numbers being characteristic of turbulence near the virial radius, while the smaller numbers pertain to the core. The simulation also predicts the existence of ordered bulk flows in the core with $v \sim 400$ km/s on scales of several hundred kpc. In this paper we consider the observability of such fluid motions via the distortions it induces in the CMB via the kinematic SZ effect, as well as via Doppler broadening and shifting of metal lines in the X-ray spectrum. We estimate $|\Delta T/T|_{kinematic} < \text{few} \times 10^{-6}$ — at or below current limits of detectability. However, we find that an energy resolution of a few eV is sufficient to detect several Doppler shifted components in the 6.7 keV Fe line in the core of the cluster.

Subject headings: Cosmology – galaxies: clusters – X-rays: galaxies

1. Introduction

Independent lines of observational evidence show that a large fraction of nearby clusters of galaxies are dynamically young. These include detection of substructure in optical and X-ray surveys (Geller & Beers 1982; Dressler & Shectman 1988, Jones & Forman 1992), non-Maxwellian galaxy velocity distributions in clusters containing substructure (Beers, Flynn & Gephardt 1990; Pinkney *et al.* 1996), X-ray surface brightness distortions (Mohr, Fabricant & Geller 1993; Buote & Tsai 1995), and X-ray temperature substructure (Henry & Briel 1992; Markevitch *et al.* 1994). These features can be understood as the result of cluster mergers (e.g., Roettiger, Burns & Loken 1996), which are predicted in hierarchical structure formation scenarios (e.g., White, Briel & Henry 1993).

Cluster mergers induce large-scale bulk flows with velocities of order the virial velocity (~ 1000 km/s for rich clusters.) Cluster-wide turbulence will then be established in the intracluster medium (ICM) in a few turnover times of the largest eddies $\tau \sim r_{vir}/\sigma_{vir} \sim 10^9$ yr. We expect the turbulence to possess

[†]This paper was written in 2000 prior to the launch of ASTRO-E, but was never submitted or published due to the unfortunate loss of that spacecraft. We release it now without major changes in anticipation of the launch of ASTRO-E2, which should have sufficient resolution to see the effects predicted here.

¹Max-Planck-Institut für Astrophysik, Karl-Schwarzschild-Strasse 1, 85748 Garching, Germany; sunyaev@MPA-Garching.mpg.de

²Space Research Institute, Russian Academy of Sciences, Profsoyuznaya 84/32, 117810 Moscow, Russia

³Physics Department and CASS, University of California at San Diego, CA 92093, USA; mlnorman@ucsd.edu

⁴Department of Physics, University of Oxford, Keble Road, Oxford Ox1 3RH; gbryan@astro.ox.ac.uk

a Kolmogorov-like spectrum down to the dissipation scale $l_{diss} \sim l_{outer}/Re^{3/4}$, where Re is the Reynolds number. Due to the low densities and high temperatures of the ICM plasma, the Coulomb mean free path is of order 10-100 kpc, yielding the *classical* estimate $Re \sim 100$. However, the presence of a weak magnetic field will reduce transport coefficients from the Spitzer values by a factor of $\sim 1/M^2$, where $M \equiv \frac{v}{\sqrt{B^2/4\pi\rho}}$ is the Alfvén Mach number (Tao 1995). Using typical values for X-ray cluster cores(halos) of $v = 300(600)$ km/s, $n = 10^{-3}(10^{-5})$ cm $^{-3}$, and $B = 10^{-6}(10^{-8})$ G, we find $M^2 \sim 10(10^4)$. This increases the effective Reynolds number to $\sim 10^3(10^6)$, predicting dissipation scales of ~ 5 kpc(30 pc), assuming $l_{outer} = 1$ Mpc.

There are two ways to study the nature and importance of these motions (i.e., their contribution to the local pressure of the gas, mixing of the high Z elements in the cluster and their contribution to ion heating due to dissipation in the smallest scales). First, through numerical simulation of the evolution of the gas in the cluster, taking into account evolution of the gravitational potential, mergings, heating and cooling of the gas, formation of the cooling flows etc. Recently Norman & Bryan (1999) published results of such simulations. Second, to use X-ray spectroscopy missions (under construction now and under consideration) to measure the real distribution of velocities in rich clusters of galaxies. We are excited by the progress in the energy resolution of AXAF and XMM (with X-ray grating), ASTRO-E (with X-ray bolometers). CONSTELLATION and XEUS projects planned for the launch by NASA and ESA in the middle of the next decade would have 1-2 eV energy resolution in the whole band from 1 to 7 keV. Such energy resolution will permit measurements of velocities as low as 50-100 km/sec, more than an order of magnitude lower than the sound speed in rich clusters of galaxies.

In this paper we use the published data on the velocity distribution in a simulated rich cluster of galaxies (Norman & Bryan 1999) to demonstrate that the observations of X-ray lines with high energy resolution would open the new method to investigate the large scale intergalactic gas velocity distribution in clusters of galaxies. It is important for us that we are dealing with heavy elements and especially with iron, which is 56 times heavier than hydrogen and therefore its thermal velocity (and corresponding thermal line broadening) is 7.5 times lower than the proton thermal velocity. This opens the way to measure subsonic turbulent velocities.

Observations and simulations have shown that the gas in the cluster is not isothermal (Markevitch *et al.* 1998, Frenk *et al.* 1999). Using lines of different ions and elements we get an opportunity to measure the velocity distribution in the regions with different temperatures in the same line of sight. We note that there is only one way to compete with X-ray observations to measure cluster gas motions. This is to observe the microwave hyperfine structure lines of heavy ions (for example 3.03 mm line of Lithium-like iron-57)(Sunyaev & Churazov, 1994). These lines are analogous to 21 cm line of hydrogen. Unfortunately they are not sufficiently bright, therefore it is better to observe the broadening of X-ray lines.

2. The Numerical Simulation

We have simulated the formation of an adiabatic X-ray cluster in an $\Omega = 1$ universe. The initial spectrum of density fluctuations is CDM-like with a shape parameter of $\Gamma = 0.25$ (Efstathiou *et al.* 1992). The cluster itself is a 3σ fluctuation at the center of the box for a Gaussian filter of 10 Mpc radius. We use a Hubble constant of 50 km/s/Mpc and a baryon fraction of 10%. This cluster is the subject of a comparison project between twelve different simulation methods, the results of which can be found in Frenk *et al.* (1999).

The evolution of gas and dark matter is computed using a new method to numerical cosmology:

adaptive mesh refinement (AMR). AMR utilizes a logical hierarchy of finer resolution meshes in regions of the calculation which require high resolution (in our case, collapsing halos of dark matter and gas.) AMR is adaptive, automatic and recursive: an arbitrary number of sub-meshes of different levels of resolution are automatically created as the solution evolves. Within each sub-mesh, the equations of adiabatic gas dynamics are solved subject to boundary conditions interpolated from overlying coarser meshes using the piecewise parabolic method (PPM) as modified for cosmology by Bryan et al. (1995). Dark matter dynamics is solved using an adaptive particle-mesh (APM) algorithm inspired by Couchman’s (1991) algorithm. Details of the method can be found in Bryan & Norman (1997), Norman & Bryan (1999).

The simulation was initialized with two grids at two levels of refinement. The first is the root grid covering the 64 Mpc^3 triply periodic domain with 64^3 cells. The second grid is also 64^3 cells, but is only 32 Mpc on a side and is centered on the cluster. Thus, over the region that forms the cluster, we have an initial cell size of 500 kpc leading to an approximate mass resolution of $8.7 \times 10^8 M_\odot$ ($7.8 \times 10^8 M_\odot$) for the baryons (dark matter). Cells are flagged for refinement when the baryon mass exceeds $4M_{initial} \approx 3.5 \times 10^9 M_\odot$. We use a refinement factor $R = 2$, thus immediately after refinement, a refined cell’s baryon mass will be $0.5M_{initial}$. As the simulation evolves, as many as ~ 400 grids at seven levels of refinement are created, with a minimum cell size of $64 \text{ Mpc}/64 \times 2^7 = 7.8 \text{ kpc}$. Our method thus maintains mass resolution in the gas and dark matter, while providing high force resolution where needed. In this regard, we accomplish the same thing as an adaptive smoothing length SPH calculation (e.g., Navarro, Frenk & White 1995) with a less viscous, more accurate shock-capturing hydrodynamic scheme. This is a distinct advantage in simulations of cluster turbulence.

Figure 1 shows radial profiles of the spherically averaged gas and dark matter velocity dispersions in the cluster at $z = 0$. The cluster centroid is taken to be the point of maximum total density. The dark matter velocity dispersion is computed after subtracting off the mean cluster peculiar velocity inside a sphere of radius $r_{200} \approx 2.2 \text{ Mpc}$. It shows the characteristic quasi-isothermal plateau $\sigma \approx \sigma_{vir}$ for $0.05 \leq r/r_{vir} \leq 0.5$, sharply declining in the outer and inner parts of the cluster as discussed by Frenk et al. (1998). The gas velocity dispersion exhibits a different profile as the dark matter as the kinetic temperature contribution is not included. Only peculiar fluid velocities due to bulk motions or turbulence are reflected here. We compute the fluid velocity dispersions relative to the mean *fluid* peculiar velocity inside spheres of three different radii: 0.01, 0.1, and 1 r_{vir} . The curves for 0.1 and 1 r_{vir} are nearly identical, and show fluid peculiar velocities are dominated by infall for $r \geq r_{vir}$. Inside the main cluster shock at $r \approx r_{vir}$, the ICM is in a turbulent state (Bryan & Norman 1998, Norman & Bryan 1999), with σ_{gas} declining from 800 km/s to $\sim 400 \text{ km/s}$ at $r = 0.5r_{vir}$. The turbulent velocities are roughly constant inside $0.5r_{vir}$, which is the significant new result of our simulation. Visual inspection of the flowfield reveals turbulent eddies with a range of sizes 50 - 500 kpc. In addition, the flowfield in the central few hundred kpc exhibits an ordered circulation with $v \approx 400 \text{ km/s}$. Visualizations of the velocity field can be found in Norman & Bryan (1999) and at the web site <http://zeus.ncsa.uiuc.edu:8080/Xray/clusters.html>.

In the following sections, we explore whether such fluid motions are detectable.

3. Results

3.1. Kinematic and Thermal SZ Effect

A hot ICM will inverse Compton scatter the cosmic microwave background radiation, boosting photons to higher frequencies and distorting the Planck blackbody spectrum (Sunyaev & Zel’dovich 1970, 1980). In

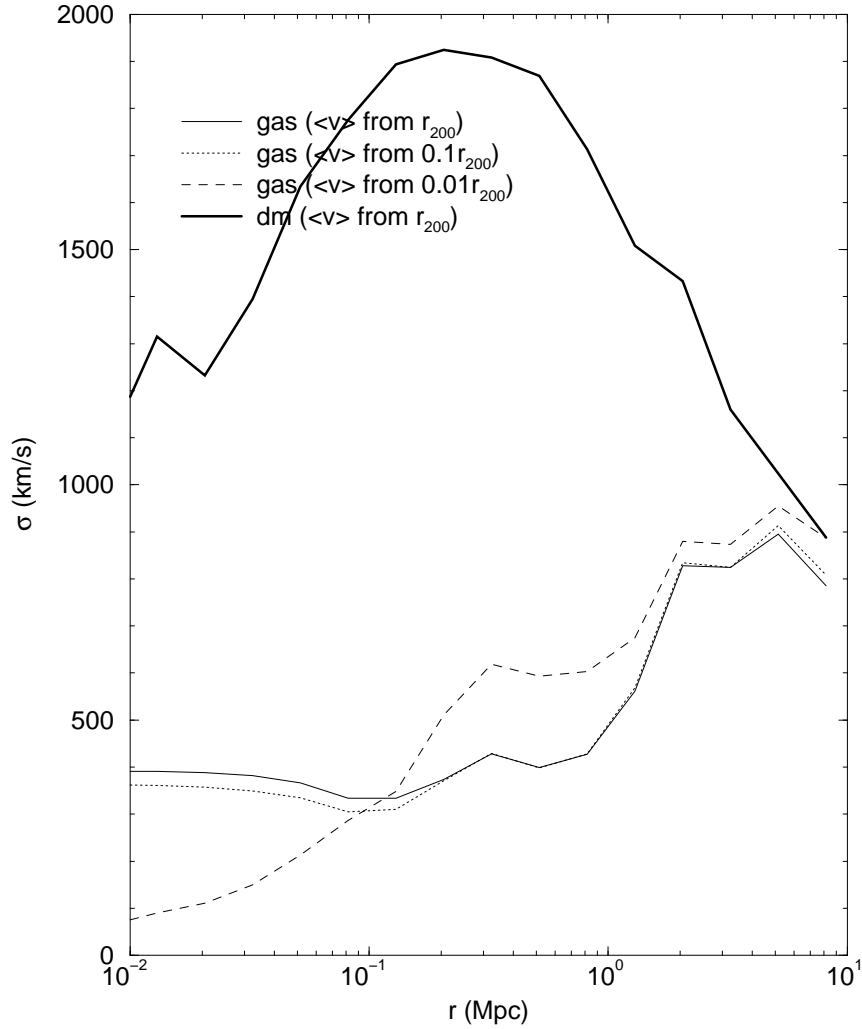


Fig. 1.— Spherically averaged profiles of gas (thin lines) and dark matter (heavy line) 3D velocity dispersions in the simulated X-ray cluster. The gas velocity dispersions are computed relative to the center-of-mass velocities inside spheres of different radii: (r_{200} (thin solid line); $0.1r_{200}$ (thin dotted line); and $0.01r_{200}$ (thin dashed line)). The plateau in $\sigma_{gas} \sim 400$ km/s for $r \leq 1$ Mpc is indicative of bulk velocities/turbulence in the cluster gas.

the Rayleigh-Jeans part of the spectrum, the temperature decrement due to this effect is $\Delta T/T = -2y$, where y is the line of sight integral of essentially the gas pressure through the ICM

$$y = \int_{-\infty}^{\infty} \frac{kT_e}{m_e c^2} \sigma_T n_e dl. \quad (1)$$

T_e , m_e , and n_e are the electron temperature, mass, and number density and σ_T is the Thompson scattering cross section. In addition to this *thermal* effect, which is insensitive to fluid motions in the ICM, there is also a *kinematic* effect, which to first order in $\frac{v}{c}$ is

$$\frac{\Delta T}{T} = -\frac{1}{c} \int_{-\infty}^{\infty} \sigma_T n_e v_{\parallel} dl, \quad (2)$$

independent of frequency. Here v_{\parallel} is the line-of-sight component of the cluster gas peculiar velocity (i.e., relative to the CMB frame.) The total temperature decrement is the sum of these two effects

$$\left(\frac{\Delta T}{T}\right)_{tot} = \left(\frac{\Delta T}{T}\right)_{thermal} + \left(\frac{\Delta T}{T}\right)_{kinematic} = -\tau_T \left[2 \frac{k \langle T_e \rangle}{m_e c^2} + \frac{\langle v_{\parallel} \rangle}{c} \right], \quad (3)$$

where τ_T is the Thompson optical depth, and $\langle T_e \rangle$ and $\langle v_{\parallel} \rangle$ are the electron density-weighted electron temperature and fluid velocity along the line-of-sight.

Because of the n_e weighting and the fact that observed X-ray clusters have monotonically decreasing temperature profiles (Markevitch et al. 1998), we expect the thermal SZ effect to be highest in the core. Figures 2a and b confirm this expectation, where we present images of the y -parameter for our simulated cluster on two spatial scales. Isocontours of y are smooth, concentric, and nearly circular, consistent with recent radio interferometric observations (Carlstrom et al. 1999). The peak value of $y \approx 10^{-4}$ is also consistent with observed values (Carlstrom et al. 1999), although our result is naturally sensitive to our assumed Ω_b .

Since v_{\parallel} is a signed quantity, the magnitude of the kinematic SZ effect will depend not only on the strength of turbulent or bulk motions in the cluster core, but also on the number of velocity reversals along the line of sight. Images of the kinematic SZ effect on two spatial scales are shown in Figs. 2c and d, obtained by integrating equation (2) along multiple lines-of-sight through the simulated cluster. One sees a reversal in $\Delta T/T$, due to the aforementioned circulation in the cluster core. Across the center of the cluster, $\Delta T/T$ changes abruptly from -4 to $+4 \times 10^{-6}$, or about 2% the magnitude of the thermal effect. Let us check this result for consistency. From equation (3), setting $k \langle T_e \rangle = 4.8$ keV (the mass weighted temperature inside r_{vir}), we deduce $\langle v_{\parallel} \rangle = 56$ km/s, about a quarter of the one-dimensional gas velocity dispersion in the core. In addition to the dominant effect due to core circulation, we can see cluster-wide fluctuations in the kinematic SZ effect image due to turbulent motions in the ICM, as well as due to a subcluster falling in at 3 O'clock in Fig. 3c. These fluctuations are at an amplitude of $\Delta T/T \approx 10^{-6}$.

The kinematic SZ effect due to cluster turbulence is just below current limits of detectability. Subtraction of background radio galaxies, which are not resolved in the BIMA and OVRO interferometers used for the current observations, introduce a systematic uncertainty of 15-25 μ K (Cooray et al. 1999) in the SZ decrement, versus our peak signal of $\sim 11 \mu$ K. Better point source subtraction using future arrays with higher spatial resolution and visibility coverage should allow us to detect the kinematic effect due to cluster mergers, turbulence and bulk flows in the ICM.

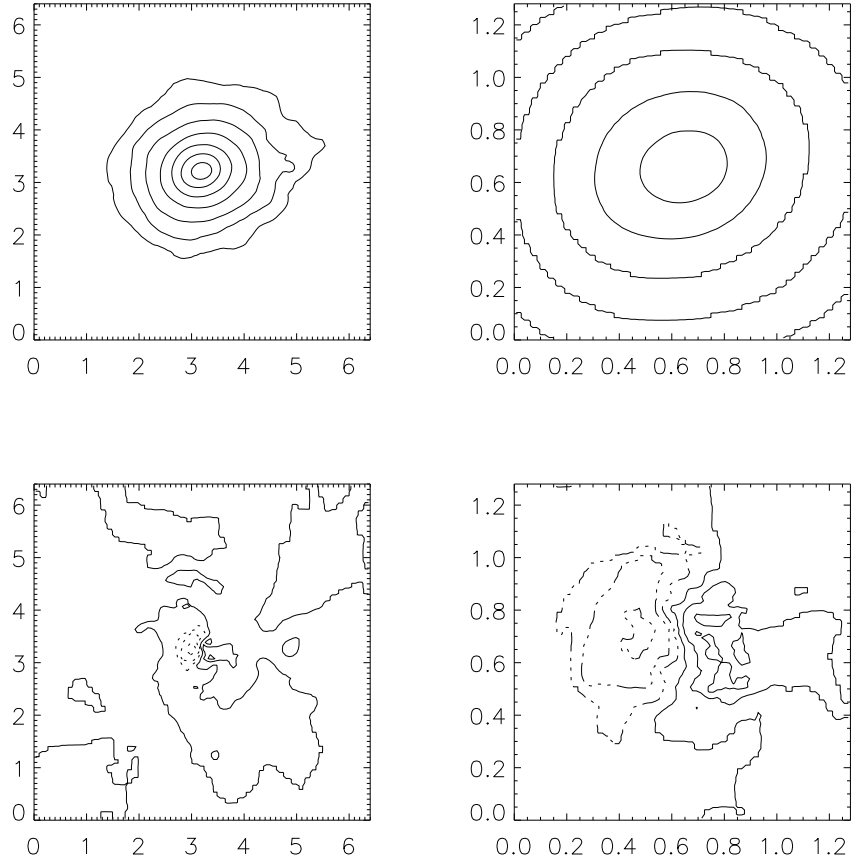


Fig. 2.— Top: the SZ thermal y-parameter for a region 6.4 Mpc (left) and 1.2 Mpc (right) on a side. Bottom: the SZ kinematic effect, in terms of $\Delta T/T$. The y contours are logarithmically spaced: 1, 2, 4, 8, 16, 32 and 64×10^{-6} for the large (6.4 Mpc) region and 4, 8, 16, 32 and 64×10^{-6} for the small (1.2 Mpc) region. The kinematic contours are -4, -2, 1, 0, 1, 2, 4×10^{-6} and the negative contours are dotted.

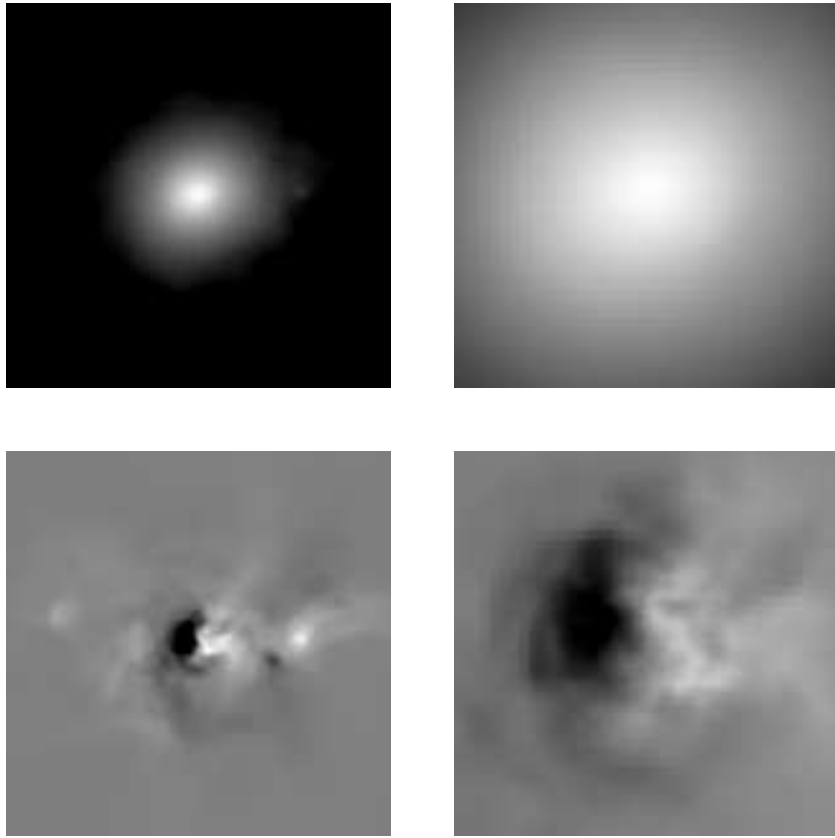


Fig. 3.— Same as previous figure, but an image representation. The y -parameter is log-scaled from 10^{-6} to 10^{-4} (both images), and the kinematic $\Delta T/T$ goes from -2 to $+2 \times 10^{-6}$ on for the large (left) image and -4 to $+4 \times 10^{-6}$ for the small image (1.2 Mpc, on the right).

3.2. Doppler Broadening and Shifting of Metal Emission Lines

The radial component of the thermal velocity of iron ions is ~ 130 km/s for 5 keV temperature. Radial turbulent velocities decrease from ~ 500 km/s at the virial radius to ~ 250 km/s in the core (Fig. 1). In addition, we have radial infall of gas and subclusters beyond the virial radius with $|v_r| > 1000$ km/s, and an ordered circulation with $v \sim 400$ km/s in the core. Thus we might expect to see in a high resolution X-ray spectrum multiple components in iron emission lines with Doppler shifts of magnitude ΔE 2-6 times the thermal width, or $\pm 6 - 18$ eV. We examine this possibility quantitatively in Fig. 4.

To isolate the effects of gas motions on X-ray line spectra, we plot the distribution of emission for an infinitely thin line with intensity proportional to $n_e^2 f(T_e)$ versus radial velocity relative to the cluster rest frame (top axis) or energy (bottom axis) for nine lines-of-sight through the simulated cluster. The line emissivity is assumed to be proportional to $n_e^2 f(T_e)$. In Fig. 4 we set $f(T_e) = 1$ for simplicity; below we construct more realistic spectra. Each l.o.s. is normalized to the total amount of flux in the line, and that normalization (relative to the line through the cluster center) is shown in the upper right-hand corner.

In the absence of bulk motions and turbulence, the plot should show delta function emission at $\Delta E = 0$. Instead we see multiple components spread over the range of energies estimated above. The asymmetric profiles seen at negative impact parameters are the result of a large sub-clump falling into the cluster at high speed. The profiles at impact parameters $b \geq 0$ show a roughly symmetric plateau of components over the range ± 15 eV, with the exception of a strong peak at $b = 0, \Delta E = -5$ eV caused by fluid circulation in the core. These components will be observable with order 1 eV spectral resolution, although point out that each l.o.s. is pencil-thin and that a real observation will be the (flux-weighted) average of many of these. The net result I imagine will be a much broader line with large sub-clumps moving at high speed showing up more clearly.

We now investigate what a realistic spectrum would look like, including the effects of thermal broadening, Doppler broadening and shifting due to fluid motions, and temperature effects along the l.o.s. Fig. 5 shows the 6.702 keV iron line as predicted by a Raymond-Smith code. We assume a constant iron abundance. The lines-of-sight are identical to Fig. 4. The dashed line shows the effect of thermal broadening only, while the solid line shows the full effect of thermal plus bulk motions. The emission is not normalized in this plot, as can be seen from the different scales at left. The absolute scale is arbitrary as we have not defined the cross-section of the line of sight.

Again, the infalling sub-cluster is visible as a shifted maximum, particularly in the $b = -0.3$ plot. At $b = 0$ and $+0.15$, the spectrum is turbulently broadened to several times its thermal width. Discrete subcomponents are still visible. Finally, the second peak seen at 6.685 keV is actually another iron line (in fact there are a whole series at lower energy, but this is clearly the strongest). The energy resolution in this plot is much higher than any planned mission, but it is evident that 4 eV resolution (such as that planned for ASTRO-E2) would be enough to see these nonthermal features,

4. Discussion and Conclusions

The preceding results suggest that X-ray spectroscopy is the most promising approach in the near term to detect bulk motions and turbulence in X-ray clusters. Therefore we focus our discussion on these possibilities.

Our hydrodynamical calculations show that the dynamics of cluster formation in a CDM-dominated

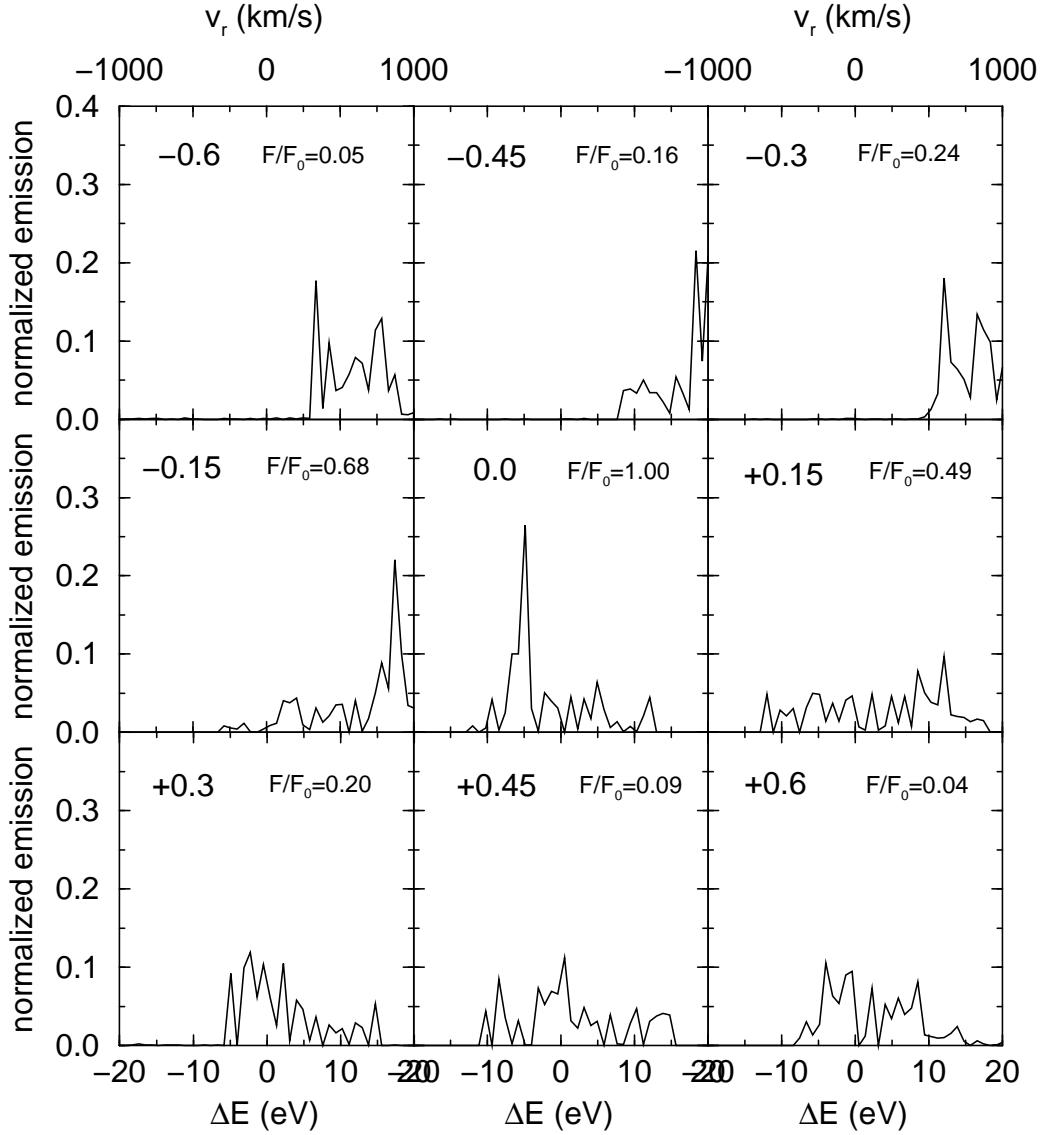


Fig. 4.— The normalized X-ray emission versus Doppler shift in eV along nine lines of sight through the simulated X-ray cluster. The corresponding radial velocities are given at the top of the plot. The impact parameter in Mpc for each l.o.s is given at upper left in each panel. The flux F in units of the central flux F_0 is given at upper right in each panel.

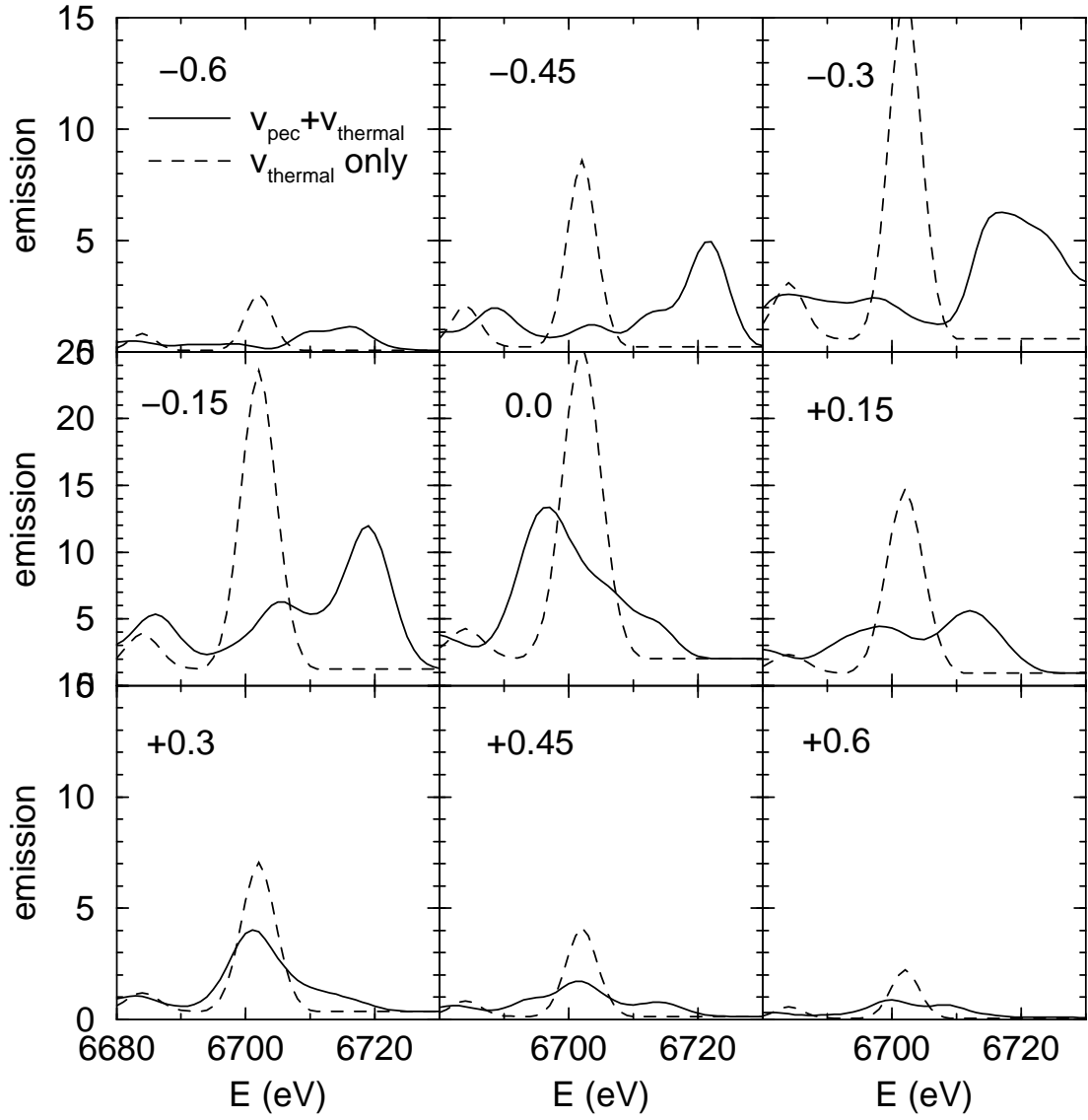


Fig. 5.— Synthetic Fe line spectra along nine lines of sight through the simulated X-ray cluster. The dashed lines are computed assuming thermal broadening only, whereas the solid lines include both thermal broadening and Doppler shift.

model produce cluster-wide turbulence and ordered bulk flows in the ICM which are strong enough to be detected in the cluster core in high resolution X-ray spectra. Due to the small thermal broadening of emission lines from heavy elements, these are the most promising probes. We have calculated a synthetic spectrum of the well-separated 6.702 keV emission line of iron which shows strong turbulent broadening and shifting of the line into multiple components over a range $\Delta E \sim \pm 15$ eV. How reliable is this result? Our finite numerical resolution in the core (~ 15 kpc) artificially cuts off the turbulent spectrum at this scale. Thus our simulation underestimates turbulent broadening due to microturbulence which could possibly eliminate discrete, Doppler shifted components. However, we have seen that some components are caused by ordered motions in the core, as well as infalling sub-clusters, and our resolution is adequate to predict these features with some confidence. A second effect not included in our synthetic spectrum is finite angular resolution, which would average over components making spectra more featureless. Thus, we expect X-ray spectra with a resolution of a few eV will see metal lines whose widths are dominated by turbulent broadening, with possibly a few components reflecting bulk motions in the core. This implies that temperature measurements from line widths will be difficult or impossible, as they will be dominated by turbulent broadening. Fig. 5 demonstrates this is true, not only in the center, but out to several core radii. However, since the turbulent velocity scales with the virial velocity of the cluster, line widths will probe the depth of the potential well.

Our predictions are based on a numerical simulation which makes a number of simplifying physical assumptions about the thermal and dynamic properties of the gas which may not reflect conditions in real X-ray clusters. For example, we ignore radiative cooling, which is important in the majority of real X-ray clusters at low redshift. In the simplest models radiative cooling in dense cluster cores lead to centrally directed cooling flows and lower central temperatures. There is some observational support for these models (Fabian 1994). However, the velocity and temperature structure in the center of a cooling flow cluster is likely to be considerably more complicated, especially if the medium is turbulent or recovering from a recent merger. It is clear from our results that high angular and spectral resolution X-ray spectroscopy will be a powerful tool to probe the physical nature of cooling flows clusters. We can imagine that turbulence provides the perturbations which, when amplified by thermal instability, yield a two-phase medium in cooling flows. Lines of S and Ar would be brighter in the cooler gas. Mapping the cluster in these lines would be very revealing. We also assume the electron and ion temperatures are in LTE. Recently, Chieze *et al.* (1998) have shown via 3D simulations that this is a poor assumption near the virial radius. Since the line emissivity is sensitive to the electron temperature, while the line widths in the absence of turbulent broadening are a function of the ion temperature, one could *in principle* determine both with sufficiently accurate observations. However, the low emission measure and high level of turbulence we find at large radii would make this measurement difficult if not impossible.

Acknowledgements MLN would like to thank the gracious hospitality of Simon White at the Max-Planck-Institut für Astrophysik where this work was done, and the Alexander von Humboldt Foundation for financial support during my stay. The numerical simulations were carried out on the SGI/CRAY Origin2000 system at the National Center for Supercomputing Applications, University of Illinois at Urbana-Champaign. This project is partially supported by NSF grant AST-9803137 and NASA grant NAGW-3152.

REFERENCES

- Beers, T. C., Flynn, K., Gebhardt, K. 1990, *AJ*, 100, 32
- Bryan, G.L. and Norman, M.L. 1997. in *Computational Astrophysics*; 12th Kingston Meeting on Theoretical

- Astrophysics, eds. D. Clarke & M. West, ASP Conference Series Vol. 123, 363
- Bryan, G.L. and Norman, M.L.. 1998. *Ap. J.*, 495, 80
- Bryan, G.L., Norman, M.L., Stone, J.M., Cen, R. and Ostriker, J.P. 1995. *Comput. Phys. Comm.*, **89**, 149
- Buote, D.A. & Tsai, J.C. 1995. *Ap. J.*, 452, 522
- Carlstrom, J. E.; Mohr, J. J.; Reese, E. D.; Holder, G. P.; Leitch, E. M.; Joy, M. K.; Grego, L.; Patel, S.; Holzzapfel, W. L. 1999. *BAAS*, 194, 5801
- Chieze, J.-P.; Alimi, J.-M.; Teyssier, R. 1998. *Ap. J.*, 495, 630
- Cooray, A. R.; Carlstrom, J.E.; Grego, L.; Holder, G. P.; Holzzapfel, W. L.; Joy, M.; Patel, S. K.; Reese, E. 1999. in “After the Dark Ages: When Galaxies were Young (the Universe at $2 \leq z \leq 5$)” eds. S. Holt & E. Smith. AIP Press, Washington DC, 1999, p. 184
- Couchman, H. M. P. 1991. *Ap. J. Lett.*, 368, 23
- Dressler, A. & Schectman, S.A. 1988. *AJ*, 95, 985
- Efstathiou, G., Bond, J. R. & White, S. D. M. 1992. *MNRAS*, 258, 1
- Fabian, A. C. 1994. *ARA&A*, 32, 277
- Frenk, C.S., White, S.D.M., Bode, P., Bond, J.R., Bryan, G.L., Cen, R., Couchman, H.M.P., Evrard, A.E., Gnedin, N., Jenkins, A., Khokhlov, A.M., Klypin, A., Navarro, J.F., Norman, M.L., Ostriker, J.P., Owen, J.M., Pearce, F.R., Pen, U.-L., Steinmetz, M., Thomas, P.A., Villumsen, J.V., Wadsley, J.W., Warren, M.S., Xu, G. and Yepes, G. 1999. *Ap. J.*, 525, 554
- Geller, M. J.; Beers, T. C. 1982. *PASP*, 94, 421
- Henry, J. P.; Briel, U. G. 1993. *Advances in Space Research*, vol. 13, no. 12, p. (12)191-(12)198
- Jones, C. & Forman, W. 1992. in “Clusters and Superclusters of Galaxies”, NATO Advanced Science Institutes (ASI) Series C, Volume 366, Ed. A. C. Fabian, Dordrecht: Kluwer, 49
- Loken, C., Norman, M.L., Nelson, E., Burns, J.O., Bryan, G., & Motl, P. 2002. *Ap. J.*, 579, 571
- Markevitch, M., Forman, W.R., Sarazin, C.L. & Vikhlinin, A. 1998.
- Markevitch, M., Yamashita, K., Furuzawa, A. & Tawara, Y. 1994. *Ap. J. Lett.*, 436, 71 *Ap. J.*, 503, 77
- Mohr, J.J., Fabricant, D.G. & Geller, M.J. 1993. *Ap. J.*, 413, 492
- Navarro, J.F., Frenk, C.S. & White, S. D. M. 1995. *MNRAS*, 275, 720
- Norman, M.L. & Bryan, G.L., 1999. in *Numerical Astrophysics 1998*, eds. S. Miyama & K. Tomisaka, Astrophysics & Space Science Library Vol. 240, (Kluwer, Boston), 19
- Norman, M.L. & Bryan, G.L. 1999. in *The Radio Galaxy Messier 87*, eds. H.-J. Roeser & K. Meisenheimer, Lecture Notes in Physics No. 530, (Springer, Heidelberg), 106
- Pinkney, J., Roettiger, K., Burns, J. O. & Bird, C. M. 1996. *Ap. J. Supp.*, 104, 1

- Roettiger, K., Burns, J.O. & Loken, C. 1996. *Ap. J.*, 473, 651
- Sunyaev, R. & Churazov, E. 1994. *MNRAS*, 297, 1279
- Sunyaev, R. A. & Zeldovich, Ya. B. 1970. *Ap&SS*, 7, 3
- Sunyaev, R. A. & Zeldovich, Ya. B. 1980. *ARA&A*, 18, 537
- Tao, L. 1995. *MNRAS*, 275, 965
- White, S. D. M., Briel, U. G. & Henry, J. P. 1993. *MNRAS*, 261, L8